Quaternary International xxx (xxxx) xxx–xxx

Contents lists available at ScienceDirect

Quaternary International

journal homepage: www.elsevier.com/locate/quaint

Magnetostratigraphic and chronostratigraphic constraints on the Marathousa 1 Lower Palaeolithic site and the Middle Pleistocene deposits of the Megalopolis basin, Greece

Vangelis Tourloukis[a,*], Giovanni Muttoni[b], Panagiotis Karkanas[c], Edoardo Monesi[b], Giancarlo Scardia[d], Eleni Panagopoulou[e], Katerina Harvati[a]

[a] Palaeoanthropology, Senckenberg Centre for Human Evolution and Palaeoenvironment, Eberhard Karls Universität Tübingen, Rümelinstr. 23, 72070, Tübingen, Germany
[b] Dipartimento di Scienze della Terra, Università degli Studi di Milano, via Mangiagalli 34, I-20133, Milano, Italy
[c] The Malcolm H. Wiener Laboratory for Archaeological Science, American School of Classical Studies at Athens, Soudias 54, 10676, Athens, Greece
[d] Instituto de Geociências e Ciências Exatas, Universidade Estadual Paulista, Rio Claro, SP 13506-900, Brazil
[e] Ephoreia of Palaeoanthropology-Speleology of Greece, Ardittou 34b, 11636, Athens, Greece

ARTICLE INFO

Keywords:
Megalopolis
Greece
Middle Pleistocene
Magnetostratigraphy
Lithic artifacts
Palaeoloxodon antiquus

ABSTRACT

We investigated the magnetostratigraphy of the Megalopolis basin in central Peloponnese, Greece, which encompasses a record of Pleistocene lacustrine and lignite-bearing sedimentation, where lithic tools stratigraphically associated with remnants of an almost complete skeleton of *Palaeoloxodon antiquus* were recently found at the Marathousa 1 site. A magnetic polarity reversal was observed within a ~10 m-thick lignite seam at the base of the (exposed) stratigraphic sequence, and it was interpreted as a record of the Brunhes/Matuyama boundary (0.78 Ma). Assuming that lignite seams were deposited generally under warm and humid climate conditions, this finding is in agreement with data from the literature indicating that the Brunhes/Matuyama boundary occurs within warm Marine Isotope Stage (MIS) 19. We then attempted to correlate the remainder of the lacustrine and lignite-bearing intervals above the Brunhes/Matuyama boundary to a standard oxygen isotope record of Pleistocene climate variability. Two age models of sedimentation were generated: according to preferred option #1, the artifact-bearing stratigraphic units of the Marathousa 1 site should have an age between ~0.48 Ma and ~0.42 Ma, while according to alternative option #2, the archaeological layers would have an age between ~0.56 Ma and ~0.54 Ma. Option #1 is at present considered the preferred option as it is in closer agreement with preliminary post-IR IRSL and ESR dates from the Marathousa 1 site. This age model has been exported to other areas of the Megalopolis basin, where additional archaeological and/or palaeontological sites could be present, by means of correlations to lithostratigraphic logs derived from commercial drill cores taken in the 1960s and 1970s for lignite exploitation.

1. Introduction

The Megalopolis basin, located in central Peloponnese, Greece, is a tectonic half-graben filled with Neogene to Holocene continental sediments (Vinken, 1965) (Fig. 1A). The Pleistocene portion of this sequence, which is the object of this study, includes the Marathousa and Megalopolis Members of the ~200 m-thick Choremi Formation. The Marathousa Member (Mb) is characterized by lacustrine clay, silt and sand intervals alternating with lignite seams (Fig. 1B and C), while the Megalopolis Mb comprises fluvial deposits (Vinken, 1965; Nickel et al., 1996; Sakorafa and Michailidis, 1997; Siavalas et al., 2009; van Vugt et al., 2000).

The Marathousa Mb includes the recently discovered Marathousa 1 (MAR-1) Lower Palaeolithic site (Fig. 1C; Panagopoulou et al., 2015; Harvati et al., 2016, 2017). Remains of a virtually complete skeleton of *Palaeoloxodon antiquus* were found at the contact between stratigraphic units UA3 and UA4 in association with lithic artifacts. This horizon includes also remains of cervids, bovids, micromammals, turtles, and birds (Konidaris et al., 2018), while the lithic assemblage is composed of well-preserved flakes and flake fragments, retouched tools, core fragments and debris (Tourloukis et al., 2018). The stratigraphic and spatial association of artifacts and fossils (notably, elephant bones), as well as the presence of bone modifications, suggests the involvement of hominins in the exploitation of these animal carcasses (Konidaris et al.,

* Corresponding author.
E-mail address: vangelis.tourloukis@ifu.uni-tuebingen.de (V. Tourloukis).

https://doi.org/10.1016/j.quaint.2018.03.043
Received 22 January 2018; Received in revised form 15 March 2018; Accepted 26 March 2018

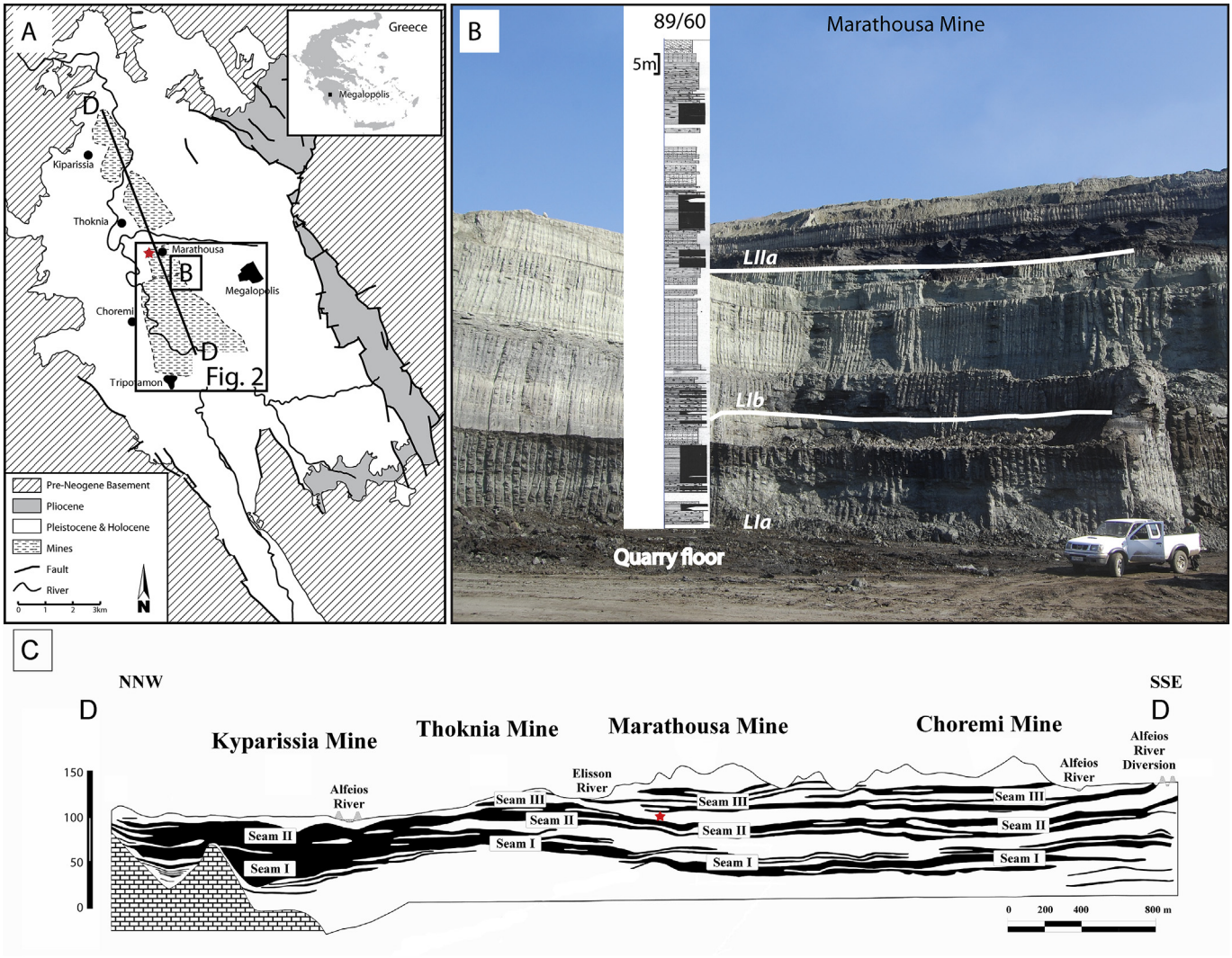

Fig. 1. (A) Geological map of the Megalopolis basin in central Peloponnese, Greece, modified from van Vugt et al. (2000). (B) Picture of Marathousa quarry wall stratigraphy placed next to drill core 89/60. (C) Cross-section D-D across the main lignite mines of the Megalopolis basin, showing the Marathousa Member stratigraphy and the stratigraphic position of the Marathousa 1 archaeological site (MAR-1); modified from Siavalas et al. (2009): Fig. 3a.

2018; Giusti et al., 2018; Panagopoulou et al., 2015; Harvati et al., 2016, 2017).

In addition to MAR-1, the limnic sediments of the Marathousa Mb have also yielded rich faunal assemblages, including a hominin tooth (Sickenberg, 1975; Harvati, 2016), as well as microfossils and micro- and macrobotanical records (e.g. Vinken, 1965; Melentis, 1965; Hiltermann and Lüttig, 1969; Nickel et al., 1996; Okuda et al., 2002). The palynological, macrobotanical, paleontological and archaeological records of the Marathousa Mb, characterized by exceptional preservation conditions in a continuous and rhythmic alternation of lithological cycles, make Megalopolis a reference basin to study the palaeolithic, palaeoecological and palaeoclimatic evolution of the eastern Mediterranean during the Pleistocene.

1.1. The chronology of the Marathousa Mb: current state of the art and open issues

Recent post-infrared Infrared Stimulated Luminescence (post-IR IRSL) and Electron Spin Resonance (ESR) age determinations indicate that the age of MAR-1 should fall between ~ 400 and ~500 ka BP (Blackwell et al., 2016; Jacobs et al., 2018). This age window, if confirmed, would make MAR-1 the oldest archaeological site in Greece and one of the oldest open-air Palaeolithic sites in the Balkans and southeastern Europe (Tourloukis and Harvati, 2018).

These new promising chronological results need however to be placed within the broader biochronological and magnetochronological framework of the Marathousa Mb based on (sometimes debated) data from the literature. A faunal assemblage presumably deriving from the Marathousa Mb was attributed by Sickenberg (1975) to the Early Biharian (approximately corresponding to the mid portion of the Early Pleistocene), based on correlations with other European faunal assemblages (e.g. Ponte Galeria, Voigtstedt, Petralona). Later, an attribution to the "uppermost part of the Villanyian" (i.e. early portion of the Early Pleistocene) was suggested on the basis of the presence of *Mimomys rex* and the absence of *Microtus* (Benda et al., 1987: 134). In a more recent study (van Vugt et al., 2000), biostratigraphic data from four faunal assemblages of micromammals were used to attribute the lower part of the Marathousa Mb (i.e. Lignite Unit I; for the various lignite units, see below) to "a late Early Biharian or a Late Biharian age", while it was suggested that, in the upper part of the Member, "the sedimentary cycles II and III have a Late Biharian age" (i.e. Lignite Units II and III, respectively; van Vugt et al., 2000: 79), implying a late Early to early Middle Pleistocene age for these units. These uncertainties indicate that the biostratigraphic dating of the Marathousa Mb needs to be better defined. Indeed, van Vugt et al. (2000: 78) noted that "the biostatigraphical position of the four faunal assemblages is, however, not very

clear"; notwithstanding, they asserted (2000: 79) that their biostratigraphic conclusion "confirms that the paleomagnetic reversal indicated in deposits in between cycle I and II can be correlated with the Matuyama-Brunhes transition". In particular, van Vugt et al. (2000) conducted a magneto- and cyclostratigraphic study of the Marathousa Mb and, together with the paleontological data, they provided a chronological bracketing for the Marathousa Mb between ~900 and ~350 ka BP, based on the stratigraphic position of the Brunhes/Matuyama boundary (780 ka), phase relationships of pollen diagrams with a reference $\delta^{18}O$ curve (see also Okuda et al., 2002), and derived astronomical tuning.

Considering the stratigraphic placement of MAR-1 below Lignite Unit II (see detailed argumentation below), the site should date to Marine Isotope Stages (MIS) 16 (broadly around 630–670 ka) if the age-model of van Vugt et al. (2000) is correct. In this age-model, however, there are certain problems with the chronological bracketing of the Marathousa Mb, as well as the chronological placement of MAR-1 in MIS 16:

1) van Vugt et al. (2000) reported unresolved normal overprinting that partially obscured the precise identification of the Brunhes/Matuyama reversal; as a consequence, the Brunhes/Matuyama boundary was placed in levels above Lignite Unit I and within a sequence of detrital sediments. However, most researchers (including van Vugt et al., 2000) agree that the Marathousa Mb detrital intervals likely correspond to cold (glacial) stages, while the lignite seams should represent warm (interglacial) periods (Nickel et al., 1996; van Vugt et al., 2000; Okuda et al., 2002). Consequently, as the broadly accepted position for the Brunhes/Matuyama boundary is within the warm stage of MIS 19 (e.g. Tauxe et al., 1996; Scardia and Muttoni, 2009 and references therein), this reversal should correlate with a lignite deposit. Hence, if the stratigraphic placement of the Brunhes/Matuyama boundary is incorrect, the entire age-model would need to be re-assessed.
2) As noted above, the biostratigraphic data provide only a very broad chronological bracketing for the Marathousa Mb.
3) The above-mentioned recent post-IR IRSL and ESR dates from the site of MAR-1 provide age estimates much younger than MIS 16 for the site, thereby posing further doubts about the robustness of the available (van Vugt et al., 2000) chronological framework.

In short, as the identification of the Brunhes/Matuyama reversal is questionable, the available biostratigraphic data provide only very coarse age constraints, and recent optical dating assays do not seem to fit well into the current age-model (van Vugt et al., 2000), then the chronological framework of the Marathousa Mb needs to be re-examined and refined.

1.2. The chronology of the Marathousa Mb: beyond the current state of the art

To address these issues and place more refined constraints on the chronology of the Marathousa Mb and the MAR-1 site, our study focused on the following tasks:

(1) new paleomagnetic analyses were conducted in order to clarify the stratigraphic position of the Brunhes/Matuyama boundary (780 ka or 0.78 Ma; time scale of Lourens et al., 2004 used throughout) and establish the magnetostratigraphy of the Marathousa Mb.
(2) The lithostratigraphic sequence of the Marathousa Mb was studied and a detailed argumentation about the stratigraphic position of MAR-1 is presented. A number of commercial cores have been drilled from the 1960s up to the 1980s to assess the lateral and vertical extension of lignites. We had access to the stratigraphic logs of several drill cores (e.g. 75/60, 76/60, 25/58, 24/58, 89/60, the latter also displayed as an example in Fig. 1B; see Fig. 2 for the geographic locations of drill cores) that we used in conjunction with our own field observations to reconstruct the general evolution of the Megalopolis basin around the MAR-1 archaeological site. We had also access to the geological cross-sections generated in the 1960s and 1970s to assess the stratigraphy of the basin (Gold, 1961; Becker-Platen, 1964; Dreschhoff, 1965; Athanassiou et al., 1972). In addition, we logged and sampled for paleomagnetism two new stratigraphic sections named 1/2014, located ~1 km to the east of the MAR-1 archaeological site, and 2/2014, located a few km to the south of 1/2014 (Fig. 2).

Additionally, we investigated the anisotropy of magnetic susceptibility (AMS) to assess energy and flow dynamics of the MAR-1 depositional environment, thereby contributing to the discussion on the various processes that led to MAR-1 formation and preservation (see also Karkanas et al., 2018; Giusti et al., 2018).

These new analyses, implemented by valuable data from the literature (e.g., van Vugt et al., 2000; Okuda et al., 2002), were used to generate two alternative age models of sedimentation for the Marathousa Mb, obtained by means of magnetostratigraphy and correlations to Pleistocene climatic variability as revealed by a standard $\delta^{18}O$ curve from the literature (Lisiecki and Raymo, 2005).

2. Stratigraphy

The stratigraphy of the Marathousa Mb is well exposed in the Marathousa and Choremi mines where lignite of the Marathousa Mb is being extracted for energy production by the Public Power Corporation S. A. Hellas. The stratigraphy is described using our field observations at sections 1/2014 and 2/2014 located in the Marathousa and Choremi mines, respectively (Fig. 2). Section 1/2014 consists of a ~100 m-thick alternation of black lignites (L), organic matter rich silty clays (OMSC), gray silty clays (GSC), fining upward cycles of light gray sand and silt (LGSS), and fining upward cycles of light gray gravel, sand and silt (LGGSS) (Fig. 3, left panel). The lower part of section 1/2014 was studied for magnetostratigraphy (Fig. 3; see below). The 26 m-thick ancillary section 2/2014, also studied for litho-magnetostratigraphy (Fig. 4), is located in the adjacent Choremi mine and is considered correlative with the lower portion of section 1/2014.

A similar complex alternation of black lignites and gray sand-silt-clay intervals was observed and sampled for magnetostratigraphy by van Vugt et al. (2000) in two correlative sections located in the Marathousa and Choremi mines, i.e. the same mines that we sampled. As introduced earlier, these authors found evidence in the lower part of both sections for a lower reverse–upper normal magnetic polarity reversal interpreted as a record of the Brunhes/Matuyama boundary (0.78 Ma). In addition, Okuda et al. (2002) studied the pollen record of a third section straddling the Marathousa Mb; they correlated lignite seams bearing temperate oak forest taxa with warm MISs 15, 13, 11, and 9, whereas the intervening detrital beds with semi-arid steppe taxa (mainly *Artemisia*) were linked to cold MISs 14, 12, and 10. Unfortunately, neither the van Vugt et al. (2000) magnetostratigraphic sections nor the Okuda et al. (2002) pollen record could be correlated with a high degree of confidence to the MAR-1 archaeological levels or the stratigraphic sections and drill cores used to erect our stratigraphic scheme (see below).

The MAR-1 archaeological site is located at the northwestern edge of the Marathousa mine (Fig. 2). The site has yielded fossil bones and lithic artifacts found at the contact of stratigraphic units UB4 and UB5 at Excavation Area B (Fig. 5), as well as from the contact of the lithostratigraphically correlative units UA3 and UA4 at nearby Excavation Area A (see Karkanas et al., 2018, and Giusti et al., 2018, for more details on the lithostratigraphy and finds distribution at MAR-1). The artifact-bearing layers belong to a sedimentary sequence that is bounded by two lignite seams and is composed of two parts (Karkanas et al., 2018). The lower part includes a coarsening-upwards (CU)

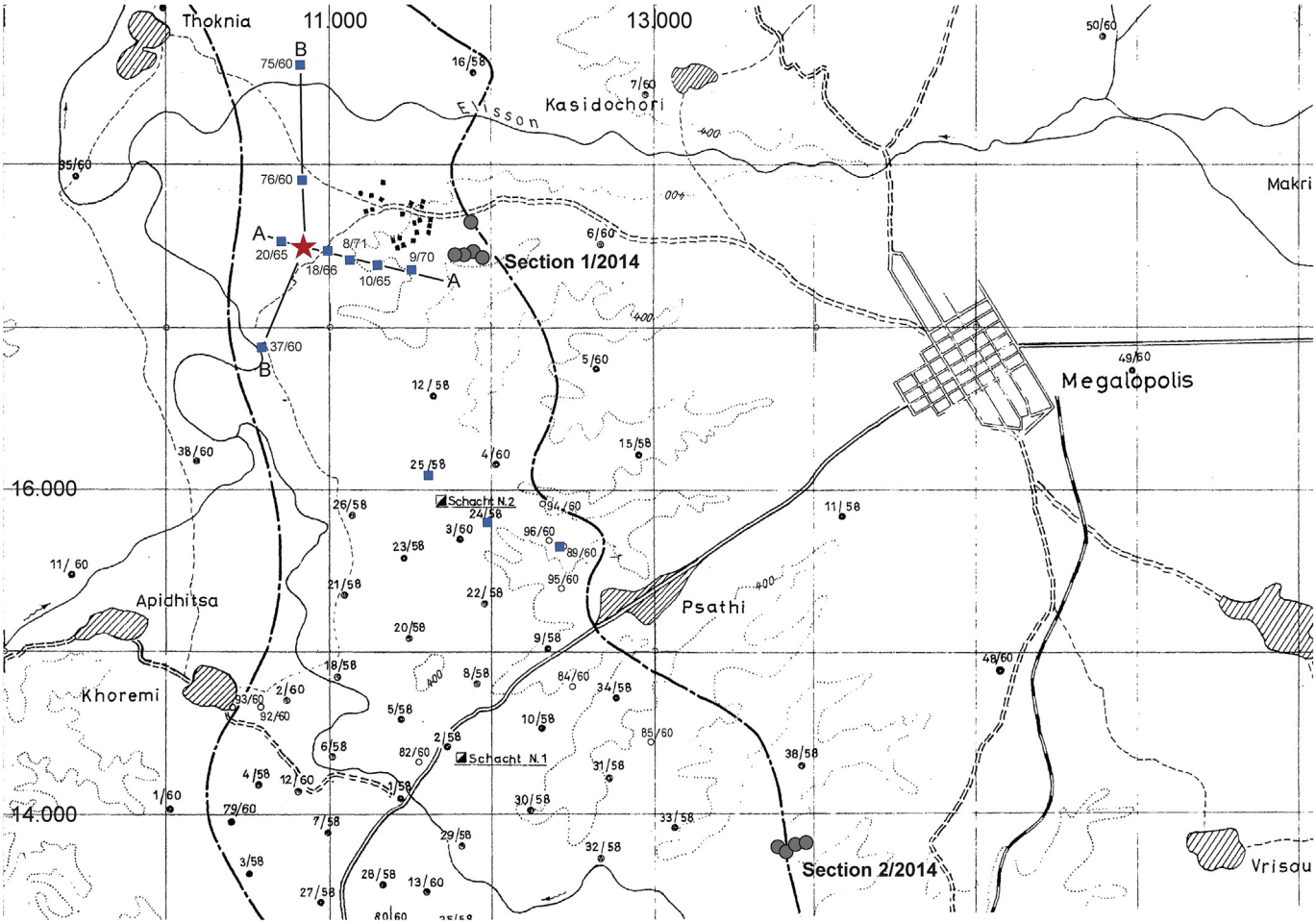

Fig. 2. Topographic map of the study area with locations of sampling sections and drill cores discussed in the text, the latter marked with rectangles. The star marks the location of the Marathousa 1 archaeological site (MAR-1). Cross-sections A-A and B-B are shown in Fig. 7A and B, respectively. Map modified from Gold (1963). (For interpretation of the references to colour in this figure legend, the reader is referred to the Web version of this article.)

sequence with massive to bedded muds and sands, which bear deformation features (slumping, liquefaction) and indicate wave or current activity. The archaeological finds are associated with a major erosional contact and most of them, including the elephant remains, lie at or close to this contact (Giusti et al., 2018); the latter represents a hiatus and an exposed surface, and marks the beginning of the upper part of the sequence characterized by fining-upwards units (FU). This upper part includes organic-rich muds and bedded sands in erosional-bounded depositional units, which represent mudflows and hyperconcentrated flows. Overall, the MAR-1 sequence points to a shallow-water environment at the shores of a lake and close to mudflat areas (Karkanas et al., 2018).

The MAR-1 sequence is sandwiched between two lignite seams (Fig. 6), which we consider to be lignite unit II (LII) and lignite unit III (LIII) as defined and described by Löhnert and Nowak (1965), and Vinken (1965). These researchers first recognized that the Marathousa Mb comprises three main lignite units (LI to LIII) separated by two thick detrital units. This subdivision was based on the observation of the stratigraphy of several commercial drill cores and has been accepted and further validated ever since by several authors (Fig. 7; Hiltermann and Lüttig, 1969; Athanassiou et al., 1972; Benda et al., 1987; Nickel et al., 1996; van Vugt et al., 2000). Our own field observations confirmed this large-scale division of the Marathousa Mb sequence. Each lignite unit can be further divided into individual seams (LIa to LIc, LIIa and LIIb, and LIIIa to LIIIc) separated by detrital levels, albeit this finer-scale subdivision does not necessarily appear in all boreholes. van Vugt et al. (2000) and Okuda et al. (2002) have considered seams LIIIb and LIIIc as separate lignite units (Lignite IV and V, respectively), but this discrepancy is irrelevant for the purposes of this work and the discussion that follows.

As anticipated, within each of the main lignite units, individual lignite seams variably alternate with detrital layers. Thus, there is a first-order cyclic pattern, where, for instance, LIIa is followed upwards by a detrital bed; LIIb is overlain by another detrital bed, and so forth; and a second-order cyclicity, where thinner lignite layers are interlayered within the detrital units. This rhythmic alternation has been attributed to astronomical periodicities (van Vugt et al., 2000): the first-order lithological cycles should represent glacial-interglacial cycles, and the second-order lignite-detritus couplets should represent intermediate climatic conditions, such as those prevailing during stadials and interstadials (for more details and a discussion, see Nickel et al., 1996; van Vugt et al., 2000; Okuda et al., 2002).

Unit LII is the most uniform of the three lignite units in terms of lateral continuity and thickness; it is also the best-exposed and most extensively quarried lignite in the Marathousa and Choremi mines. LII occurs almost always in a bipartite form: a lower 3–6 m-thick part (LIIa) and an upper 7.5 to 15 m-thick part (LIIb). Importantly, a 10 to 20 cm-thick limestone layer is intercalated in LIIb; it only occurs in areas where the base of LII is above 320 m a.s.l., i.e. mainly in the western, northern and southern parts of the Marathousa and Choremi mines, and its presence has been securely assessed in a large number of boreholes over a wide area. Consequently, this distinctive bed – informally termed here 'Franz' – has been used as a lithostratigraphic marker for the identification and correlation of lignite unit LII and in particular of

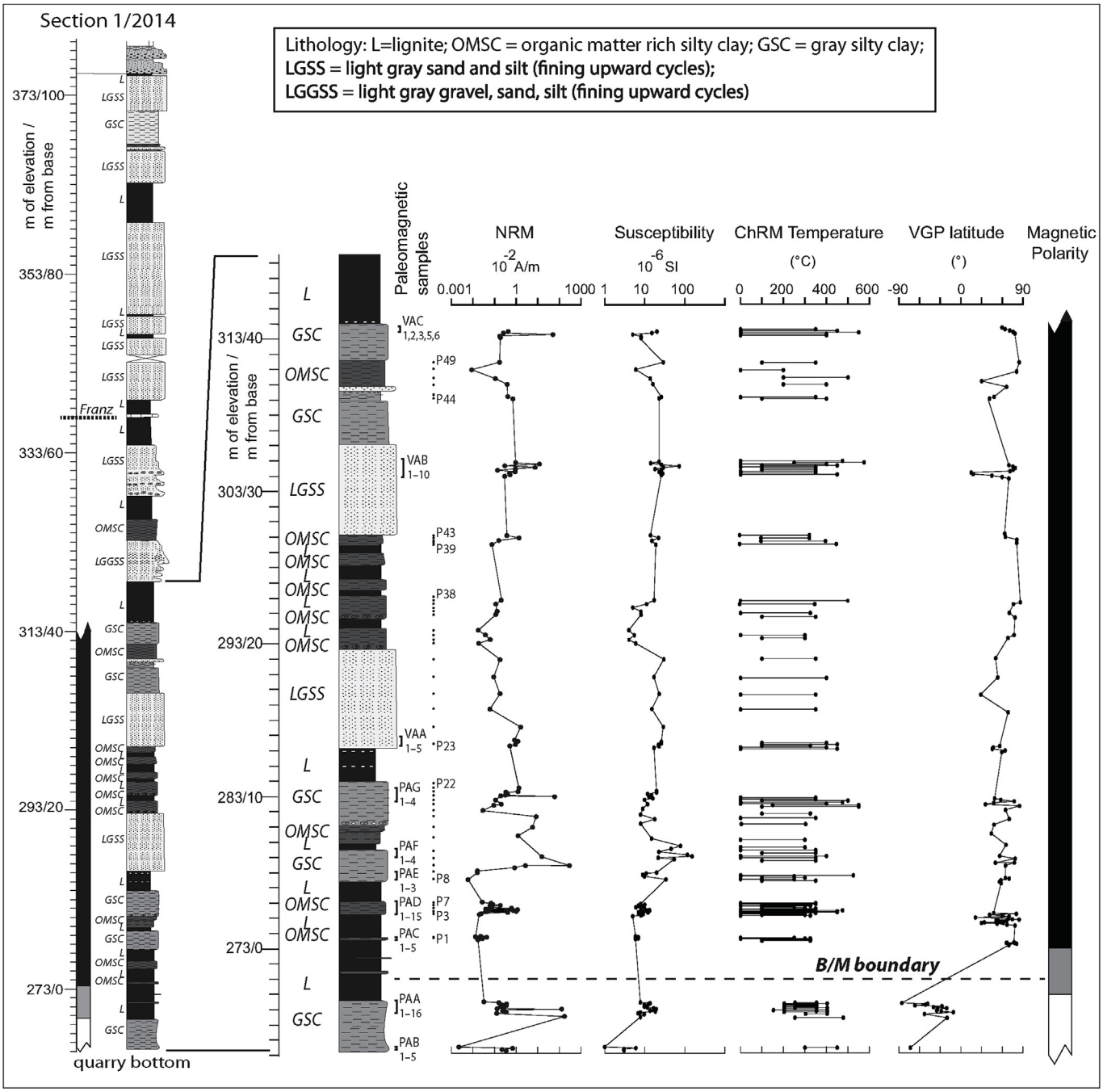

Fig. 3. Lithology log of section 1/2014 (this study) across the Pleistocene Megalopolis basin sequence at the Marathousa mine. Paleomagnetic data from the lower ~45 m of the section are as follows, from left to the right: stratigraphic position of paleomagnetic samples, natural remanent magnetization (NRM) intensity, magnetic susceptibility, the unblocking temperature spectra of the characteristic remanent magnetization (ChRM), virtual geomagnetic pole (VGP) latitudes and magnetic polarity where black is normal polarity, white is reverse polarity, and gray is main sampling gap at Brunhes/Matuyama boundary. Samples are listed next to the lithological comlumn. See text for discussion.

seam LIIb (Löhnert and Nowak, 1965; Vinken, 1965).

We place the MAR-1 site stratigraphically above LIIb and below LIII, on the basis of the following evidence:

1) the presence of the aforementioned limestone marker bed 'Franz' in the lignite seam directly underlying the MAR-1 sequence (Fig. 6, inset), which, for the considerations outlined above, would correspond to seam LIIb as evidenced from visual correlation to thicker and more complete exposures in the basin depocenter.
2) The elevation of the MAR-1 sequence at ~347–351 m a.s.l. (artifact-bearing units at ~350 m a.s.l.). Aside from deposits that are locally displaced by faults, all layers in the basin are characterized by gentle dips and, over short distances, their floors/roofs occur in relatively restricted and projectable elevation ranges. Particularly, at the western rim of the Marathousa mine (where MAR-1 is located), the base of LIIa occurs at 330–332 m a.s.l. and the base of LIIb at ~337–340 m a.s.l., while the base of LIII is consistently found above 348–350 m a.s.l. (see boreholes 75/60, 76/60, 37/60, 10/65, 18/66; Fig. 7). Hence, in the absence of faults in the vicinity of the site, the elevation of the strata can be used in conjunction with borehole data to assess the stratigraphic position of MAR-1.
3) The MAR-1 site falls clearly between the LII and the LIII in both east-

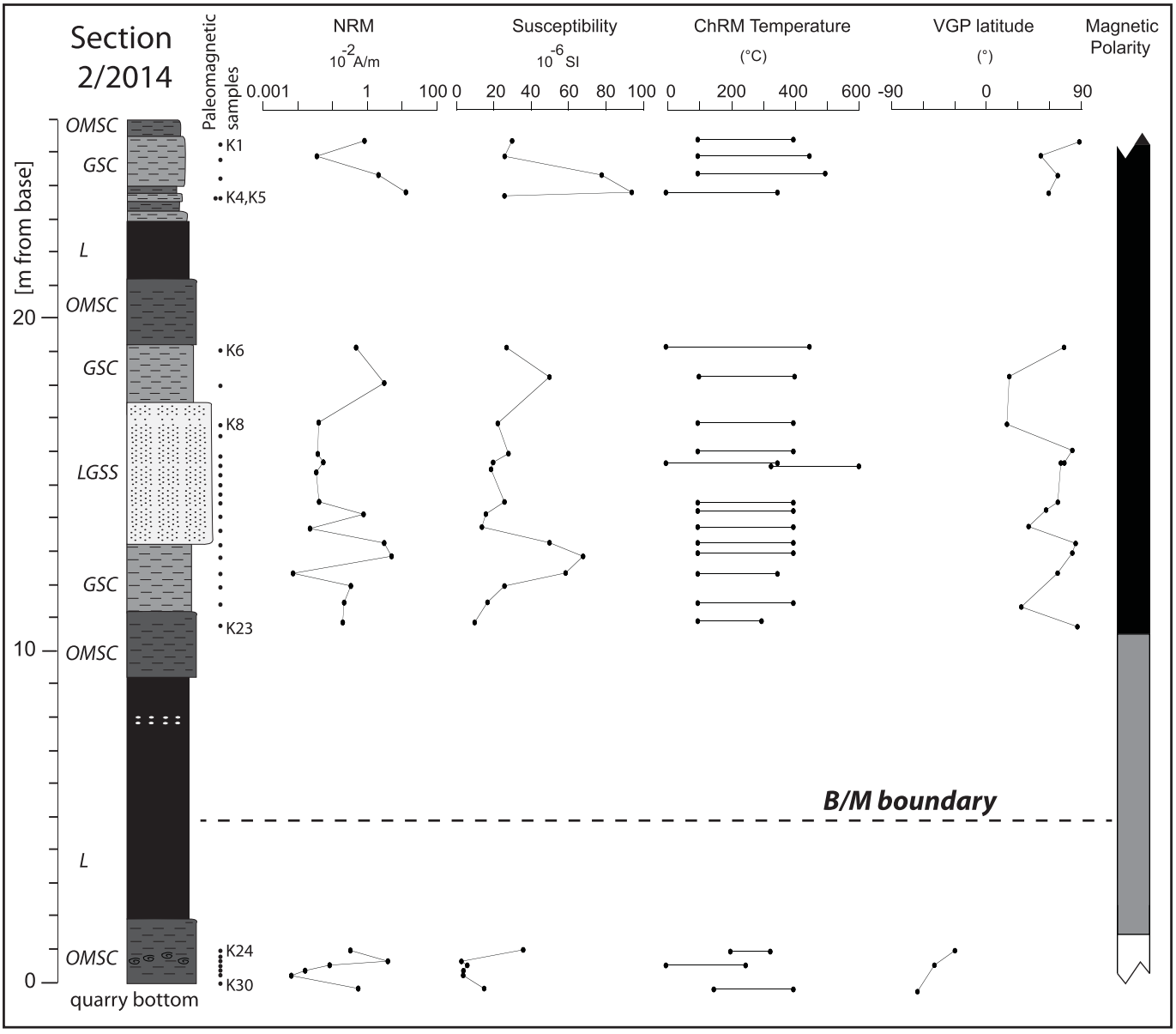

Fig. 4. Lithology log of section 2/2014 (this study) from the Choremi mine. Abbreviations of paleomagnetic data as in Fig. 3. Black is normal polarity, white is reverse polarity, and gray is main sampling gap at Brunhes/Matuyama boundary. See text for discussion.

west and north-south cross-sections (Fig. 7). Therefore, the position of the site within this particular detrital interval is verified in a three-dimensional reconstruction of the sequence and we can dismiss possible flaws due to e.g. exceptional or unmapped dipping of the layers along one of the two axis directions.

3. Paleomagnetic properties and magnetostratigraphy

Paleomagnetic sampling was performed in the more cohesive silty clays intervals; lignite intervals crumbled upon handling and could not be sampled. All paleomagnetic samples (Table 1) were cored in the field with an electric drill and oriented with a magnetic compass to obtain a total of 157 standard (10 cm^3) cylindrical specimens for section 1/2014 (Fig. 3) and 30 samples for section 2/2014 (Fig. 4). Seven cylindrical core samples were subjected to rock magnetic analyses by means of acquisition curves of an isothermal remanent magnetization (IRM) and thermal demagnetization of a three-component IRM imparted in fields of 2.5 T, 0.4 T, and 0.12 T (Lowrie, 1990). A total of 169 cylindrical core specimens were subjected to thermal demagnetization in steps of 50 °C or 25 °C using a ASC TD48 furnace, and the natural remanent magnetization (NRM) was measured after each demagnetization step with a 2G Enterprises DC-SQUID cryogenic magnetometer located in a shielded room. Standard least-square analysis (Kirschvink, 1980) was used to calculate magnetic component directions from vector end-point demagnetization diagrams, and standard Fisher statistics were used to analyze the mean component directions. Magnetic measurements were carried out at the Alpine Laboratory of Paleomagnetism (ALP) of Peveragno (Cuneo, Italy).

The intensity of the NRM varies by orders of magnitude across the various sampled lithologies from less than $0.01*10^{-2}$ A/m to more than $100*10^{-2}$ A/m (Figs. 3 and 4). The initial magnetic susceptibility co-varies with the NRM and attains values of generally less than $100*10^{-6}$ SI (Figs. 3 and 4). The IRM acquisition curves show the presence of a magnetic mineral assemblage that invariably saturates well below 500 mT (Fig. 8; samples P39, P07, K05). The thermal demagnetization of a three-component IRM is more diagnostic and reveals two main

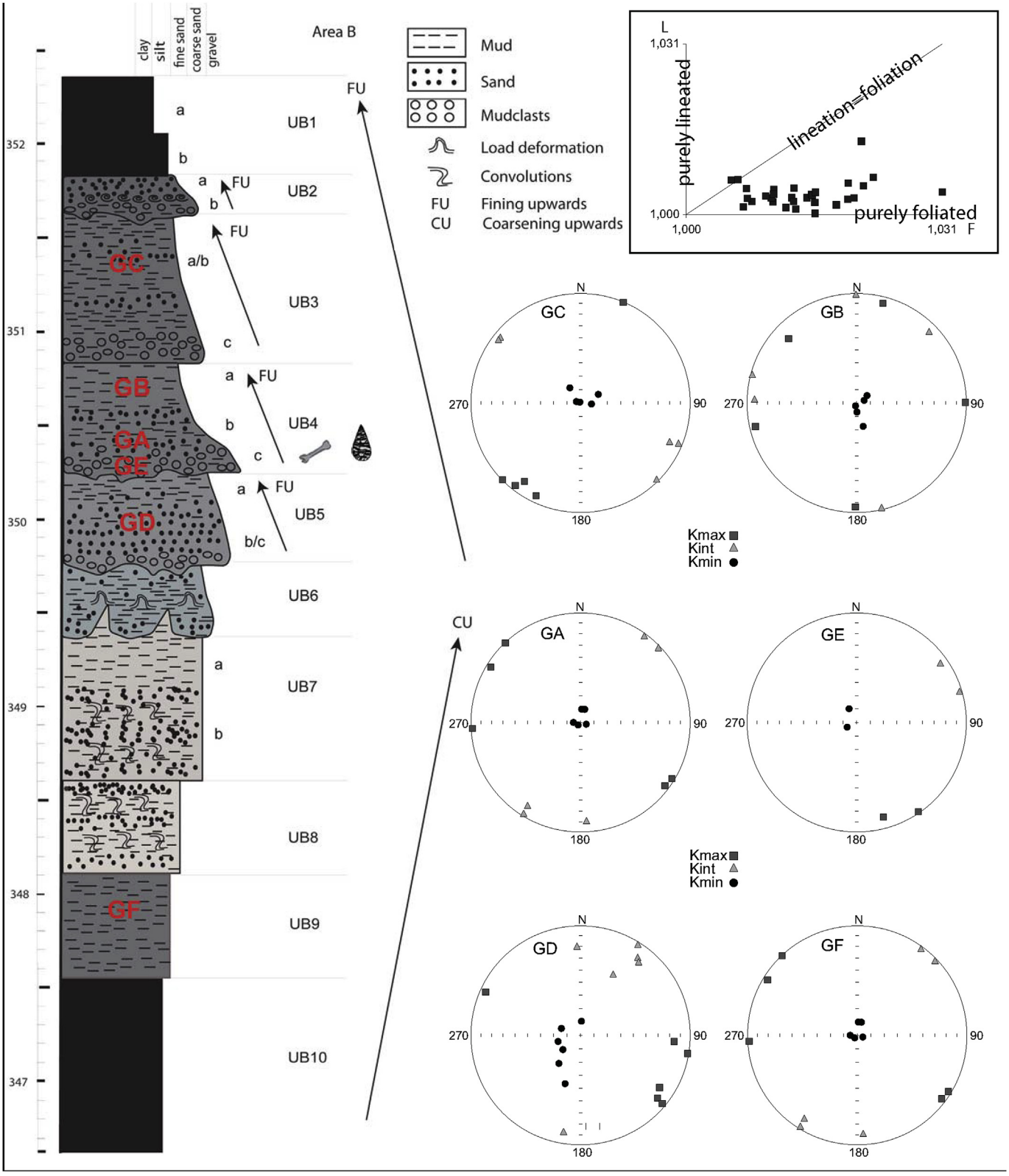

Fig. 5. Stratigraphy of the Marathousa 1 archaeological Excavation Area B (reproduced from Karkanas et al., this issue) with anisotropy of magnetic susceptibility (AMS) data. See text for discussion.

behaviors:

1. The low (0.12 T) coercivity curve shows maximum unblocking temperatures up to ~570 °C, interpreted as signaling the presence of magnetite (Fig. 8, samples P39, P07).
2. The intermediate (0.4 T) as well as the low (0.12 T) coercivity curves show a drop in intensity at around 300 °C interpreted as due to the presence of iron sulphides (Fig. 8, sample K05).

Vector end-point demagnetization diagrams show the presence of

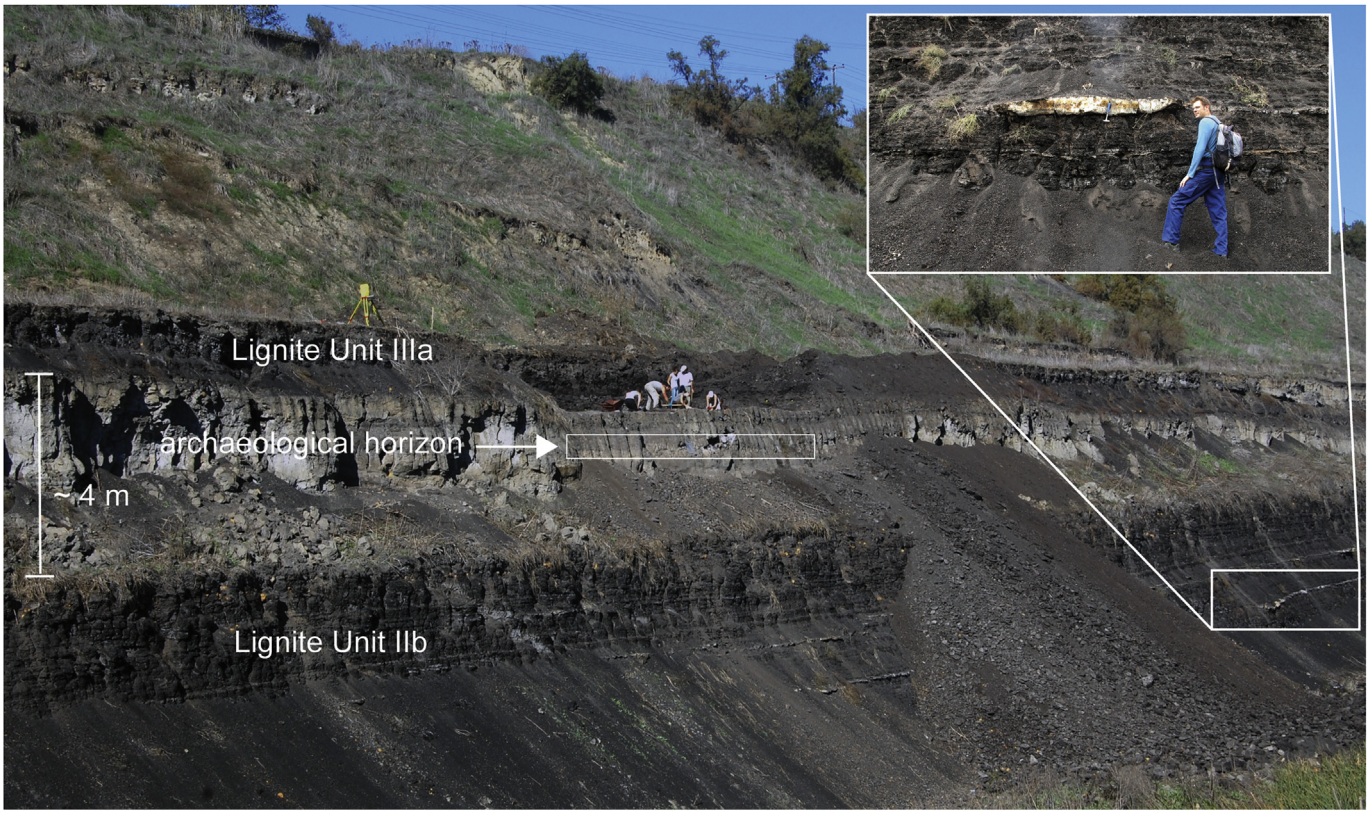

Fig. 6. Panoramic view of Excavation Area A; inset: the limestone layer (informally designated as 'Franz' in this study), which is the stratigraphic marker of Lignite Seam IIb.

characteristic component (ChRM) directions trending to the origin of the demagnetization axes and oriented to the north and down (positive inclinations) or south and up (negative inclinations) (Fig. 9A and B). These ChRM component directions were unblocked from ~100 °C to ~400 °C or up to a maximum of ~570 °C (see 'ChRM Temperature' unblocking window in Figs. 3 and 4; see also Fig. 9A and B). These antipodal ChRM component directions, obtained from a total of 95 and 21 specimens at sections 1/2014 and 2/2014, respectively, are grouped in *in situ* (geographic) coordinates around a mean of Dec. = 3.3°E, Inc. = 53.8° (k = 3, α95 = 10.3°) at section 1/2014 (Fig. 9C), and of Dec. = 358.9°E, Inc. = 58.0° (k = 7, α95 = 14.7°) at section 2/2014 (Fig. 9D). At section 1/2014, the ChRM directions are also visibly antipodal (Fig. 9C). The declination and inclination values of these ChRM component directions were used to calculate virtual geomagnetic pole (VGP) latitudes and magnetic polarity stratigraphy, with VGP latitudes approaching +90° interpreted as normal polarity and VGP latitudes approaching −90° as reverse polarity (Figs. 3 and 4). A clear upper normal-lower reverse polarity reversal is evident at Section 1 across a sampling gap of ~5 m and at Section 2 across a sampling gap of ~9 m, and is interpreted at both sections as a record of the Brunhes/Matuyama boundary (0.78 Ma).

van Vugt et al. (2000) observed a complex magnetization pattern with overprints affecting the Brunhes/Matuyama boundary at their Choremi section. In a few thermal demagnetization diagrams they observed high-temperature magnetic component directions of normal polarity that were not trending straight to the origin of the demagnetization axes, and were therefore interpreted to signal the presence of a hidden component of reverse polarity. This interpretation led them locate the Brunhes/Matuyama boundary in levels above the lowermost lignite interval and within a sequence of detrital sediments. However, it is generally agreed that the detrital intervals should correspond to cold (glacial) stages, while the lignite seams to warm (interglacial) periods (Nickel et al., 1996; van Vugt et al., 2000; Okuda et al., 2002); therefore, as the broadly accepted position for the Brunhes/Matuyama boundary is within the warm stage of MIS 19 (e.g. Tauxe et al., 1996; Scardia and Muttoni, 2009), this polarity reversal should correlate to a lignite deposit.

We did not observe the complex magnetization pattern with overprints described by van Vugt et al. (2000) and hence we used our ChRM component directions trending to the origin of the demagnetization axes to place the Brunhes/Matuyama boundary within – or at the base of – the lowermost lignite interval LI (Figs. 3 and 4; see also below).

4. Age models of sedimentation

We placed the more expanded and complete section 1/2014 together with some of the available drill core logs (75/60, 76/60, 25/58, 24/58, 89/60) as well as the MAR-1 archaeological site in a common elevation framework (Fig. 10). We attempted to place in this correlation framework also the van Vugt et al. (2000) litho-magnetostratigraphic profile from the Marathousa mine and the Okuda et al. (2002) pollen profiles from the Choremi mine, although we remind that neither their locations nor their elevations relative to the other sections and cores are known (Fig. 10).

According to this stratigraphic scheme, the main lignite units and constituent individual seams, represented by black bars on the drill core logs and stratigraphic sections, fall at slightly different elevations but appear laterally continuous and have been therefore used to erect 6 chronostratigraphic surfaces, from base to top: lignite seam LIa base, lignite seam LIb base, lignite seam LIIa base, lignite seam LIIb base, lignite seam LIIb top, lignite unit LIII base (Fig. 10).

We created two age models of sedimentation (Fig. 10) based on two different correlations of the Brunhes/Matuyama boundary and the 6 chronostratigraphic surfaces outlined above to the magneto-astrochronologically calibrated $\delta^{18}O$ benthic isotope record of Lisiecki and Raymo (2005). For the linking of the lignite-detritus alternations to

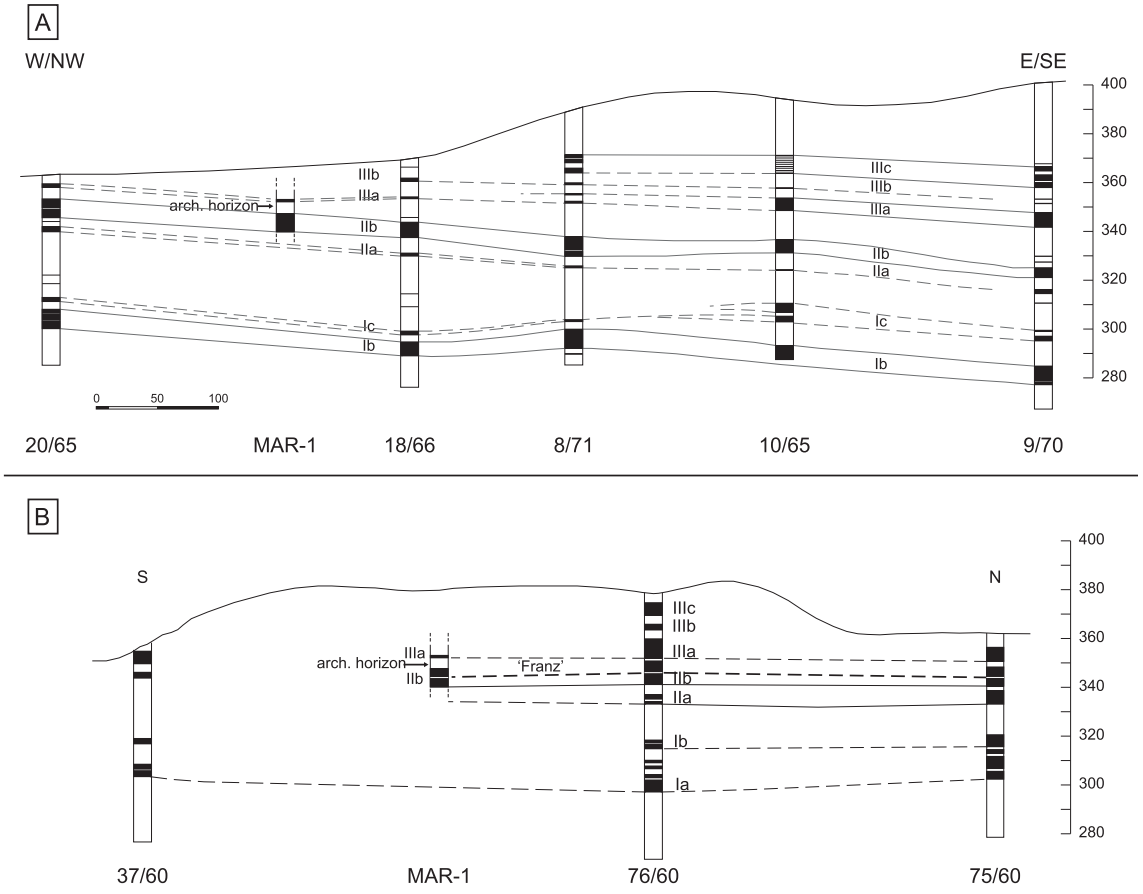

Fig. 7. (A) West/Northwest-East/Southeast and (B) North-South borehole cross-sections, showing the stratigraphic position of the Marathousa 1 archaeological site (MAR-1). See Fig. 2 for location of the cross-sections and associated drill cores. Both sections reproduced and modified from original drawings that are filed in the archive of the Public Power Corporation S.A. in Megalopolis with the following information: (A): "Profil 9, Anlage Nr. 82, Jan. 1978, Zeichn. IV/296"; (B): "Lagerstätte Khoremi Profil A, Zeichnungs-Nr. 1–7138, Anlage 14".

Table 1
Sampling sites coordinates.

Mission	Location	Site	Latitude	Longitude
Summer 2014	Marathousa mine	PAA	37.408780°	22.102002°
		PAB PAC	37.408834°	22.102003°
		PAD PAE	37.408628°	22.102813°
		PAF PAG	37.408555°	22.102937°
		VAA	37.408906°	22.102998°
		VAB	37.408659°	22.103311°
		VAC	37.408428°	22.103940°
			37.408200°	22.104287°
			37.408460°	22.104348°
			37.411079°	22.102917°
Autumn 2014	Marathousa mine	P01-P02	37.409108°	22.102606°
		P03-P06	37.409079°	22.102763°
		P07	37.409052°	22.102808°
		P08-P12	37.408997°	22.102819°
		P13-P14	37.408996°	22.102943°
		P15-P22	37.408365°	22.103973°
		P23-P28	37.408175°	22.104050°
		P29-P38	37.408261°	22.104435°
		P39-P43	37.408424°	22.104426°
		P44-P49	37.409047°	22.104221°
	Choremi mine	K01-K05	37.376066°	22.124405°
		K06-K07	37.375656°	22.124941°
		K08-K23	37.376360°	22.125754°
		K24-K30	37.376523°	22.126615°
Archaeological Site	Marathousa 1		37.410274°	22.090589°

glacial-interglacial cycles, two assumptions need first to be precluded:

1. That every individual lignite unit or seam represents a full interglacial stage (e.g., MIS15, MIS13, etc.). This scenario can hardly be considered realistic because it would stretch the Marathousa Mb well into the Late Pleistocene, which contradicts all available evidence from biochronology and radiometric assays.
2. That a single lignite unit or seam represents more than one interglacial or interstadial stage. This scenario looks also highly unlikely if we consider again the available tie points from the magnetostratigraphy, biochronology and radiometric dating of the Marathousa Mb as well as of the overlying Potamia and Thoknia Formations that have been attributed to the Late Pleistocene (e.g. Vinken, 1965).

4.1. Preferred age model option #1

Acknowledging a position for the Brunhes/Matuyama boundary (0.78 Ma) just above LIa base, we correlate LIa with MIS 19; thus, LIa base is assumed to represent Glacial Termination (GT) IX dated to ~0.79 Ma (Fig. 10). By applying the equivalence between main lignite beds and interglacials, and between main detrital intervals and glacials, we correlate LIb base, LIIa base, and LIIb base with, respectively, GT VIII (at the end of MIS 18a) dated to ~0.72 Ma, GT VII (at the end of MIS 16a) dated to ~0.62 Ma, and GT VI (at the end of MIS 14) dated to ~0.53 Ma (Fig. 10). Chronostratigraphic surface LIIb top could be less confidently resolved within the cooling trend from MIS 13 to MIS 12, and was assigned a nominal age of ~0.48 Ma, while LIII base was

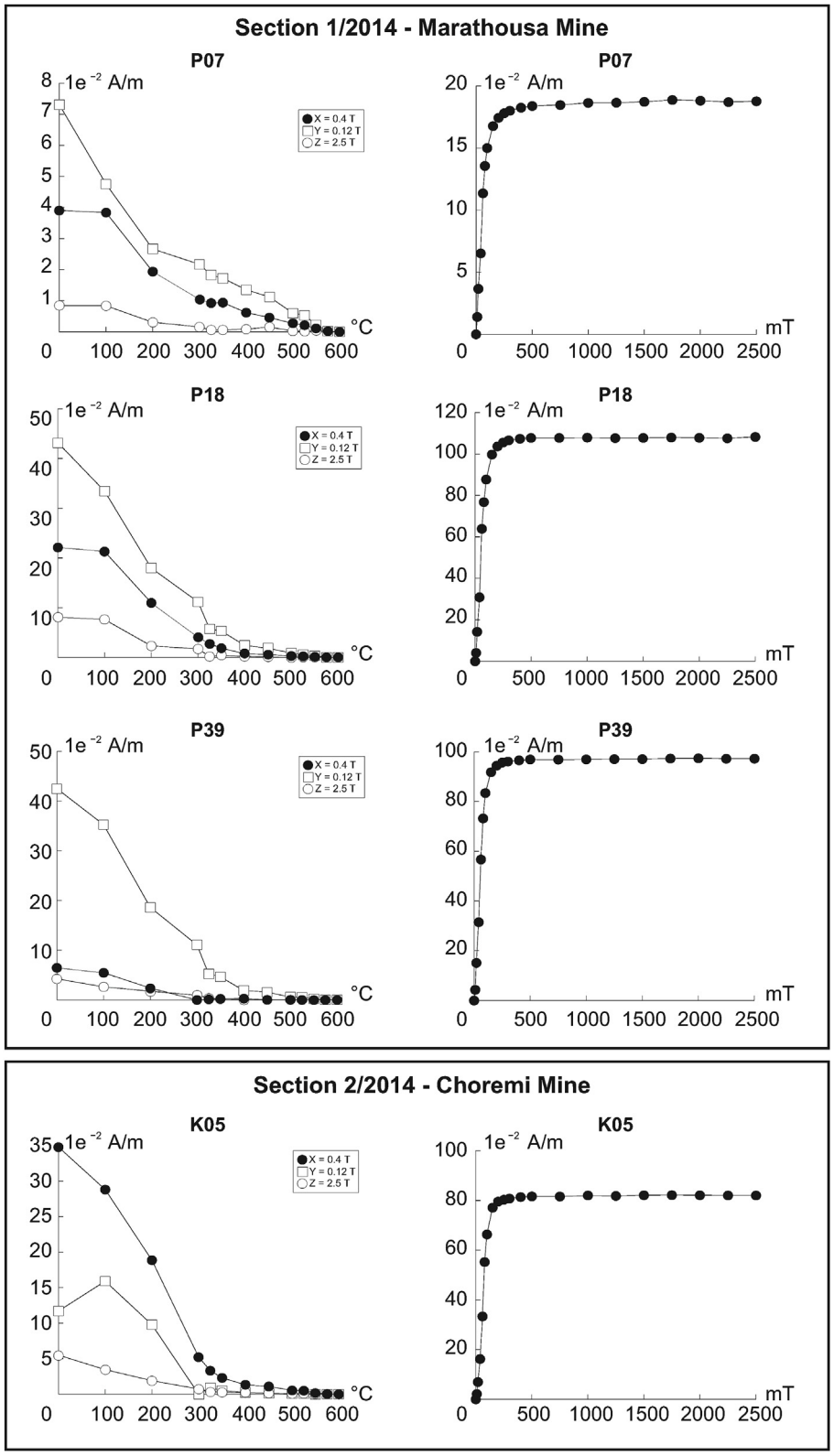

Fig. 8. Isothermal remanent magnetization (IRM) acquisition curves and thermal demagnetization curves of a 3-component IRM for representative samples from sections 1/2014 and 2/2014. For the stratigraphic position of samples, see Fig. 3 for section 1/2014, and Fig. 4 for section 2/2014.

correlated with GT V dated to ~0.42 Ma. According to this age model, the archaeological-bearing stratigraphic units (UB4c-UB5 and UA3c-UA4), located between chronostratigraphic surfaces LIIb top and LIII base, should have an age broadly comprised between ~0.48 Ma and ~0.42 Ma (Fig. 10). This chronological bracketing agrees well with recent radiometric assays: post-IR IRSL of potassium-rich feldspars dated the clastic sequence between LIIb top and LIII base between ~500 and 400 ka (Jacobs et al., 2018). ESR dating of a mollusk sample from UA2 overlying the find-bearing layers provided a minimum age for this unit at ca. 400, while five subsamples of a cervid tooth

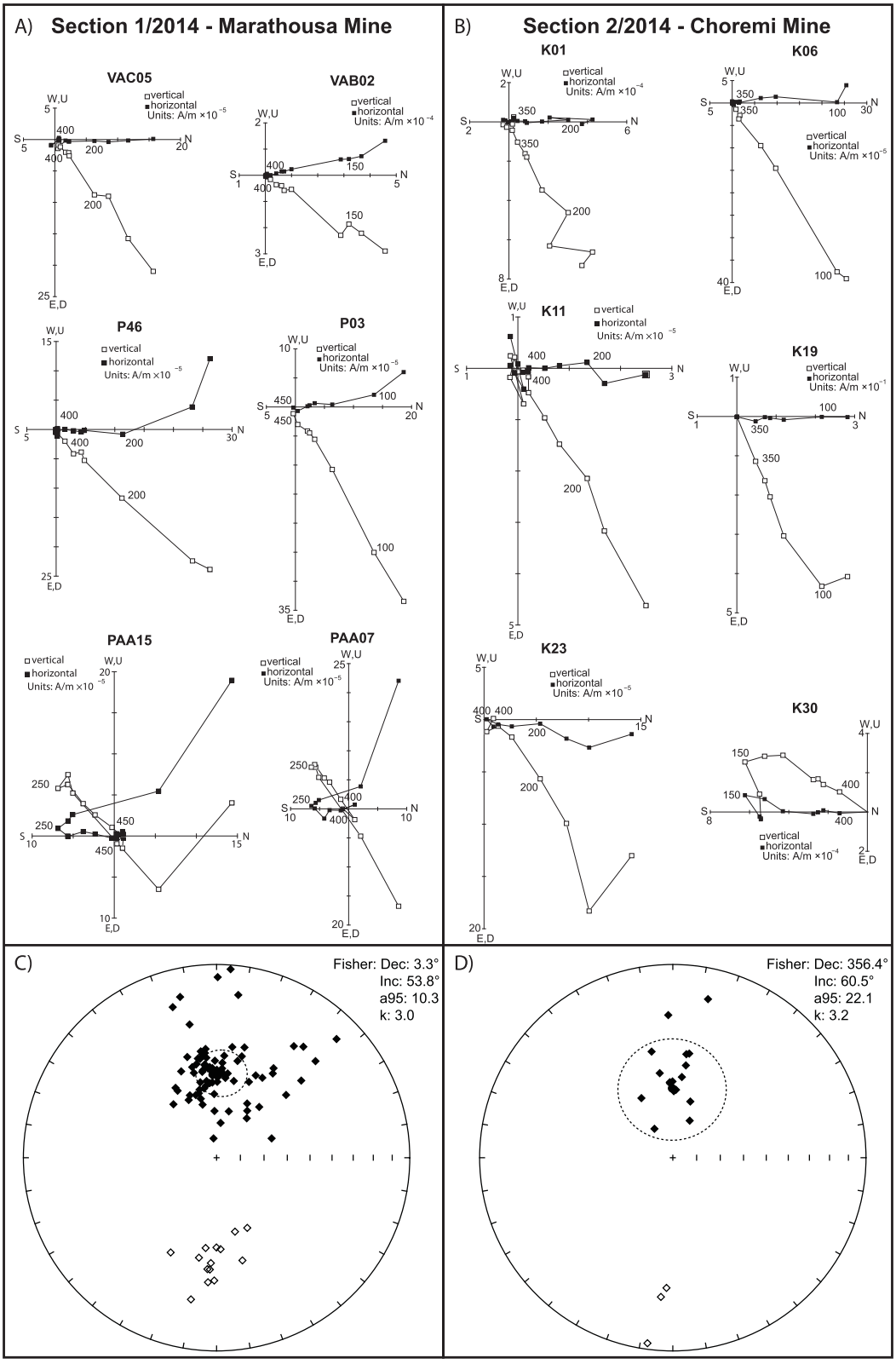

Fig. 9. Vector end-point demagnetization diagrams of representative samples from sections 1/2014 (A) and 2/2014 (B). Full symbols are projections on the horizontal plane and open symbols in the vertical plane. Demagnetization temperatures are expressed in °C. For the stratigraphic position of samples, see Fig. 3 for section 1/2014, and Fig. 4 for section 2/2014. In panels (C) and (D) equal area projection of the characteristic (ChRM) component vectors in *situ* coordinates from sections 1/2014 and 2/2014, respectively. Full symbols represent down-pointing vectors (normal polarity), open symbols represent up-pointing vectors (reverse polarity).

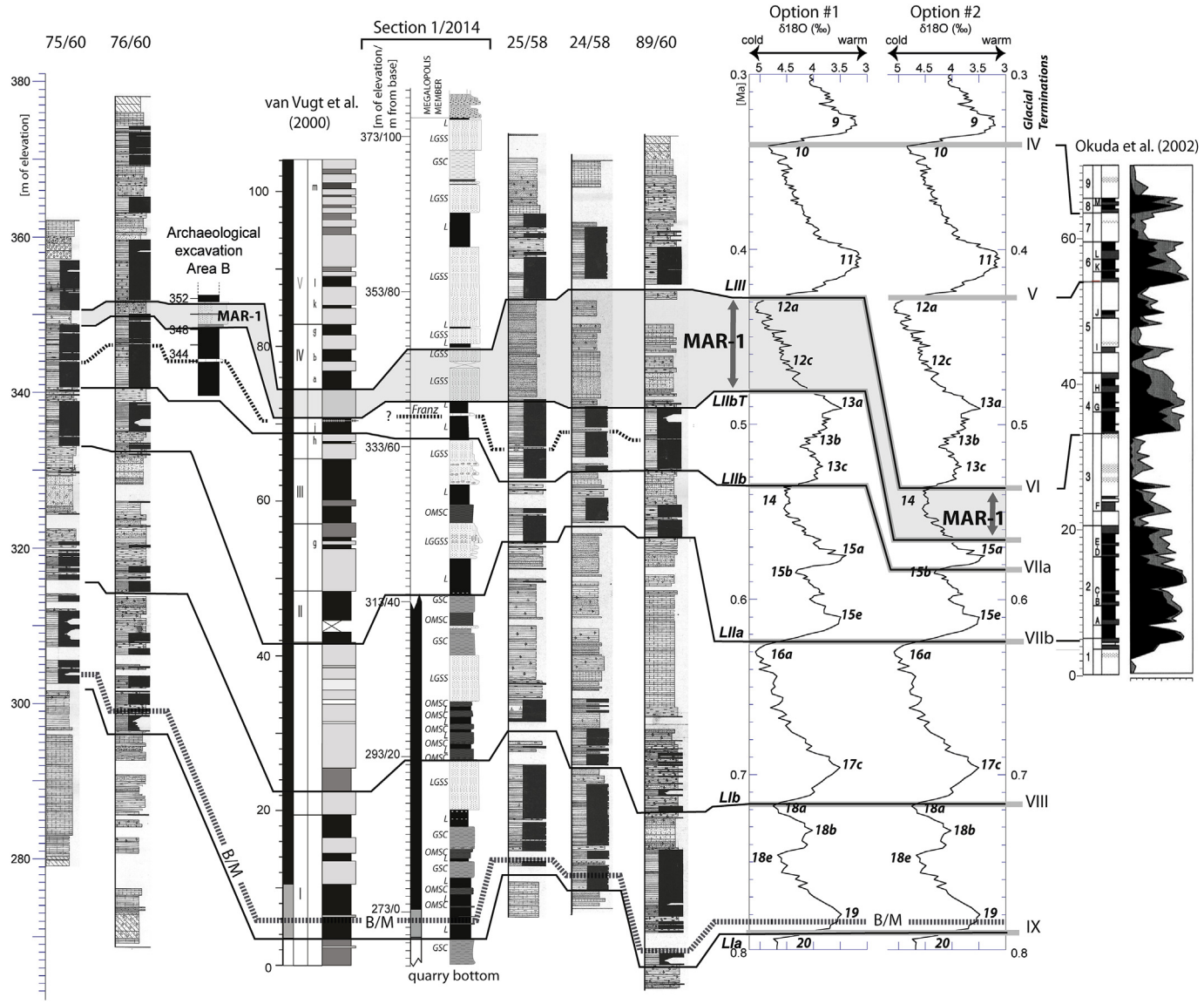

Fig. 10. Correlation scheme of a selection of commercial drill core stratigraphies and section 1/2014 of this study with the Pleistocene climatic variability represented by the $\delta^{18}O$ curve of Lisiecki and Raymo (2005). Core locations are shown in Fig. 2. Two correlation options (#1 and #2) are proposed, with option #1 considered the preferred option. See text for discussion.

excavated from UB4c (the find horizon) gave an age of ca. 500 ka (Blackwell et al., 2018). For these reasons, option #1 is at present considered the preferred option.

4.2. Alternative age model option #2

This alternative option is equivalent to preferred option #1 from LIa base (= GT IX at ~0.79 Ma) across the Brunhes/Matuyama boundary (0.78 Ma) up to LIIa base (= GT VIIb at the end of MIS 16a at ~0.62 Ma) (Fig. 10). It then departs from option #1 insofar as it assumes that LIIb base corresponds to the (minor) glacial termination at the end of MIS 15b with an age of ~0.58 Ma, LIIb top to a level within the cooling trend from MIS 15a to MIS 14 with a nominal age of ~0.56 Ma, and LIII base to GT VI at the end of MIS 14 dated to ~0.53 Ma (Fig. 10). According to this age model, the archaeological layers between chronostratigraphic surfaces LIIb top and LIII base would have an age comprised between ~0.56 Ma and ~0.53 Ma (Fig. 10).

In both age model options #1 and #2, the thick detrital interval above lignite unit LI is attributed to MIS 16; this is in accordance with pollen data showing that MIS 16 was, together with MIS 12, the most extreme glacial stage in Greece (Tzedakis et al., 2006) and we can therefore expect to be represented by thick deposits of detrital sediments. Above this thick interval, lignite unit LII should correspond to two interglacials and one intervening glacial in our preferred option #1. This attribution is in line with recent data from sedimentary records pointing to an extended, super-interglacial period encompassing MIS 15 to 13, with stage 14 being the most subdued glacial interval of the Bruhnes chron (Hillenbrand et al., 2009; Hao et al., 2015). On the other hand, our option #2 assigns this entire group of lignite-detrital-lignite triplet to a single stage, MIS 15; this scenario is in line with a recent model that views MIS 15e and 15a as two separate interglacials (Tzedakis et al., 2017). However, as mentioned above, option #1 agrees better with the available radiometric dates and remains at the moment the preferred option.

4.3. Sedimentation rates

According to the age constraints of preferred option #1, the long-term sediment accumulation rate curve calculated for section 1/2014 is ~23 cm/kyr from the section base up to chronostratigraphic surface

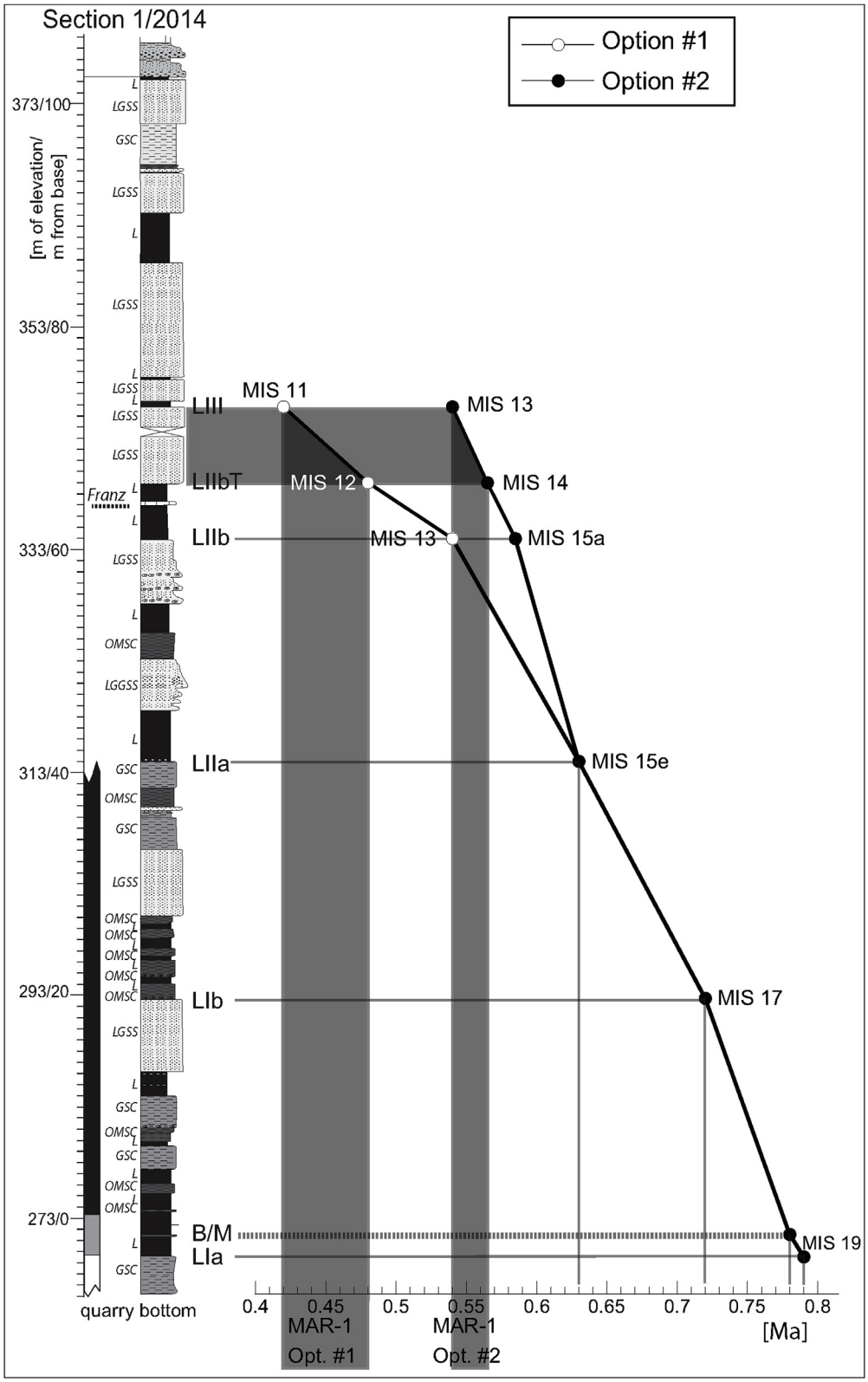

Fig. 11. Age model of sedimentation for the Middle Pleistocene part of the Megalopolis basin sequence according to preferred correlation option #1 and alternative correlation option #2. See text for discussion.

LIIb top at 66 m, and ~10 cm/kyr from LIIb top up to LIII base across the (projected) archaeological levels (Fig. 11). Instead, according to the age constraints of alternative option #2, the long-term sediment accumulation rate curve of section 1/2014 is more linearly centered around a median value of ~26 cm/kyr (Fig. 11).

In both options, drill cores 75/60 and 76/60, as well as the Excavation Area B sequence, display lower long-term sediment accumulation rates relative to section 1/2014 and correlative cores 89/60, 24/58 and 25/58; this is consistent with the general geometry of the basin, whereby cores/sections with higher sedimentation rates are

located more to the E-SE toward the basin depocenter, while cores/sections with lower sedimentation rates are located more to the W closer to the paleolake shores (see also Vinken, 1965). Overall, our values agree well with those estimated by both van Vugt et al. (2000) and Okuda et al. (2002).

5. The anisotropy of magnetic susceptibility of the MAR-1 sequence

The anisotropy of magnetic susceptibility (AMS) is a useful tool to assess depositional dynamics and characteristics, and was applied to Excavation Area B sediments. The AMS ellipsoid reflects the bulk orientation of the minimum (k_{min}), intermediate (k_{int}), and maximum (k_{max}) susceptibility axes of paramagnetic and/or ferromagnetic grains contained in a given sediment volume (usually ~10 cc). For example, phyllosilicates tend to decant in still water with their short shape axis perpendicular to the bedding plane, and as a result, an oblate mineralogical fabric develops. The AMS should reveal this fabric because, in phyllosilicates, the short shape axis broadly corresponds to the k_{min} axis, and therefore, a magnetic foliation (defined by the plane containing k_{max} and k_{int}) should develop parallel to the depositional surface; instead, when bottom currents are present, the long shape axis of elongated magnetic grains tend to line up parallel (or sometimes perpendicular) to the current direction, and the AMS should reveal this because in such grains, the k_{max} axis usually lies broadly along the flow-aligned particle length (e.g. Tarling and Hrouda, 1993; Parés et al., 2007; Felletti et al., 2016).

We sampled almost the entire sequence of MAR-1 at Area B, from the mollusk-rich UB2 down to UB9, obtaining a total of 6 sites and 28 samples (Fig. 5) that were measured for AMS with a KLY-3 Kappabridge. The lineation coefficient (k_{max}/k_{int}) is usually close to 1, while the magnetic anisotropy is essentially controlled by the foliation coefficient (k_{int}/k_{min}) that suggests the AMS ellipsoids are essentially oblate (Fig. 5, upper inset). The k_{min} axis of all samples lies invariably perpendicular to the bedding plane; samples from sites GA, GE, GD and GF show a tendency to have the k_{max} axes broadly aligned in a NW–SE direction, while the k_{max} axes of site GC appear oriented NE–SW; only at site GB the k_{max} and k_{min} axes appear dispersed in a girdle parallel to the bedding plane, indicating pure foliation (Fig. 5). These data seem to suggest that sedimentation occurred either in the presence of an aligning current (e.g., GA, GE, GD, GF) or as the result of simple gravitational settling of particles (GB).

The evidence presented here completes the interpretation based on facies and sedimentological observations that the artifact-bearing UB4 and UB5a were deposited by mudflows (Karkanas et al., 2018; Giusti et al., 2018), which, we suggest, were characterized by variable concentration and grain-aligning capacity. This overall interpretation is also consistent with the general stratigraphy of the area, whereby the thin stratigraphic interval of clastic sediments straddling the archaeological layers opens up to the SE into a much thicker clastic interval (see also Fig. 10) dominated by fining-upward sequences of turbiditic origin in what is interpreted as the deeper part of the basin. Hence, we and Karkanas et al. (2018) conclude that the archaeological units were deposited close to the western paleolake margin and were subject to sedimentation events of variable energy and density (mudflows) coming from the NW and propagating as turbidites toward the east into the paleolake depocenter (Figs. 2 and 10).

6. Discussion

In our preferred correlation scheme and age model, we assumed no significant hiatuses throughout the studied sequence. Even though small hiatuses may be present, large hiatuses (e.g. in the order of one or more glacial-interglacial cycles) are unlikely to exist considering also that the basin has always been in a depositional mode with ample accommodation space during the entire time of sedimentation of the Marathousa Mb (*cf.* Okuda et al., 2002; van Vugt et al., 2000).

The number of detrital beds, the homogeneity of the lignite seams and the thickness of either type of deposits (lignite seams, detrital beds) were controlled by the combined effects of climatic and tectonic processes. Principally, tectonics provided the accommodation space and climate served as the main triggering mechanism for sedimentation: cold stages favored erosion, transport and sediment deposition, whereas warm stages promoted pedogenesis, decreased sedimentation, lignite formation and swamp progradation. Tectonics also disrupted equilibrium conditions as we see, for instance, lignite seams being thinner close to faults. Subsidence was more pronounced to the east, where normal faults provided accommodation space for sediment accumulation, while moderate subsidence to the west allowed swamps to form; as a result, the lignite seams are thickest in the western parts of the basin and wedge out towards the east, whereas the detrital deposits are thickest in the center and eastern parts of the basin, and thin out towards the west (van Vugt et al., 2000).

Although a detailed study on the neotectonic history of the region is currently lacking, it is possible that some of the spectral variability that characterize the rhythmic deposition of the Marathousa Mb could be attributed to paleoseismicity rather than climate. Nonetheless, the palynological data (Okuda et al., 2002, placed in our correlation framework) currently provide the most robust foundations for attributing most of the observed spectral variability to fluctuations of climate through time. Lignite units are assumed to correspond to warm periods (interglacials and/or interstadials), while detrital beds to cold stages (glacials and/or stadials). This hypothesis was first suggested by Nickel et al. (1996) based on palynological data from the lowermost lignite unit (LI). van Vugt et al. (2000) and Okuda et al. (2002) conducted cyclostratigraphic and palynological studies, respectively, and confirmed this matching, arguing that the lithological cycles are driven by orbital forcing: the large-scale cycles being the result of eccentricity, while the small-scale cycles of precession (van Vugt et al., 2000). Mineralogical and coal-petrography data seem to confirm this, indicating

Table 2
Summary of the available age-models for the Megalopolis basin.

Lithostratigraphic Units	Option#1 (this study)	Option#2 (this study)	van Vugt et al. (2000)	Okuda et al. (2002)
Lignite Ia	MIS 19	MIS 19	MIS 22/21	no data
Detrital Interval 1	MIS 18	MIS 18		
Lignite Ib	MIS 17	MIS 17		
Detrital Interval 2				
Lignite Ic				
Detrital Interval 3	MIS 16	MIS 16	MIS 20 - 18	
Lignite IIa	MIS 15	MIS 15e	MIS 17	MIS 15 (13)
Detrital Interval 4	MIS 14	MIS 15d-15b		
Lignite IIb	MIS 13	MIS 15a		
Detrital Interval 5 **(MAR-1)**	MIS 12	MIS 14	MIS 16	MIS 14 (12)
Lignite IIIa	MIS 11	MIS 13	MIS 15	MIS 13 (11)

that the lithology reflects a succession of limnic conditions (detrital beds) and limno-telmatic environments (lignite seams), as a result of cold-warm oscillations (Siavalas et al., 2009).

The available age models are summarized in Table 2. According to the astronomical tuning of van Vugt et al. (2000), the sequence from lignite unit LI up to lignite unit LIII (seam LIIIc?) dates to ~900–350 ka; the MAR-1 site, which we place stratigraphically between LII and LIII, chronologically falls in this scheme within MIS 16. In the age model of Okuda et al. (2002), the sequence from LII up to LIIIc dates to ~650–300 ka, and in this scheme the MAR-1 stratigraphic level corresponds to MIS 14. Note that Okuda et al. (2002) offer an alternative age-model that agrees better with their single ESR date and places the MAR-1 level inside MIS 12 (Table 2, numbers in parenthesis).

Further research is needed to test and refine the age model presented here, as well as to narrow-down the chronological bracketing of the MAR-1 archaeological site, which is currently one of the oldest open-air palaeoanthropological sites in southeastern Europe. The Megalopolis basin represents the most promising area for investigating the Lower Palaeolithic of Greece (Tourloukis, 2010: 113) in a continuous stratigraphic record spanning several glacial-interglacial cycles. This unique record provides high-resolution stratigraphic data, which are extremely valuable for assessing the imprint of climatic oscillations on terrestrial ecosystems, as well as for investigating phase-relationships between marine and continental data-sets.

7. Conclusions

In this study, we reached the following achievements:

1. We correlated several commercial drill core logs and two new outcrop sections straddling the Marathousa Mb of the Choremi Formation in the Megalopolis basin of Greece.
2. We placed the recently discovered Marathousa 1 (MAR-1) archaeological site within this general correlation scheme.
3. By using litho-magnetostratigraphy and correlation with a standard $\delta^{18}O$ record from the literature, we generated two age models of sedimentation (options #1 and #2) for the Marathousa Mb based on six independent chronostratigraphic surfaces.
4. We investigated the anisotropy of magnetic susceptibility of sediments from the MAR-1 site and evaluated palaeo-flow dynamics, thereby contributing new data for assessing the prevailing site formation processes.

Based on these achievements, we conclude that:

1. According to preferred option #1, the archaeological levels of the MAR-1 site should have an age broadly comprised between ~0.48 Ma and ~0.42 Ma, in broad agreement with preliminary post-IR IRSL and ESR dates (Jacobs et al., 2018; Blackwell et al., 2016, 2018), while according to alternative option #2, the archaeological horizon should have an age comprised between ~0.56 Ma and ~0.53 Ma.
2. The lacustrine sequence of the Marathousa Mb from the lowermost lignite unit LI and up to the first detrital interval inside lignite unit LIII dates from ~780 to ~340 ka.
3. At the Lower Palaeolithic site of MAR-1, the sediments in which the cultural material is embedded were deposited close to the paleolake shores, in a proximal environment characterized by mudflow events of variable energy and density that evolved toward the paleolake depocenter into fining-upward turbiditic sequences.

Acknowledgements

This research was supported by the European Research Council (ERC StG no. 283503 “PaGE”: Paleoanthropology at the Gates of Europe: Human evolution in the southern Balkans; and ERC CoG 724703, “Human evolution at the crossroads” awarded to K. Harvati). We are grateful to the excavation teams that worked at the Marathousa 1 site and particularly to Dr. G. Tsartsidou and I. Sifogeorgaki for their help with the sampling and the logging. We thank the Ministry of Culture, the authorities of the Peloponnese Prefecture and the Municipality of Megalopolis for their support throughout this work. We are indebted to the Public Power Corporation S. A. Hellas for providing us the numerous drill logs and cross-sections, as well as for all their help in the field. We would also like to thank two anonymous reviewers for their comments and corrections, which helped to improve the manuscript. G.M. and E.M. were supported by a grant from *Fondo Scavi Archeologici – Università degli Studi di Milano*.

References

Athanassiou, A., Kallergis, G., Kaperonis, N., 1972. Geological and deposit investigation of Marathousa lignite field (Megalopolis). Bull. Geol. Soc. Greece 9 (2), 1–36.

Becker-Platen, J.-D., 1964. Geologische Untersuchungen im Becken von Megalopolis, Arkadien. Unpublished Diploma thesis. Reinischen Friedrich-Wilhems-Universität, Bonn.

Benda, L., van der Meulen, A.J., Meyer, K.-J., van de Weerd, A., 1987. Biostratigraphic correlations in the eastern mediterranean Neogene, 8: calibration of sporomorph- and rodent-associations from the Megalopolis basin (peloponnesus, Greece). Newsletters Stratigr. 17 (3), 129–141.

Blackwell, B.A.B., Singh, I., GopalKrishna, K., Chen, K.K., Sakhrani, N., Tourloukis, V., Karkanas, P., Florentin, J.I.B., Panagopoulou, E., Harvati, K., Skinner, A., 2016. ESR dating the fossil-bearing layers at the Marathousa 1 site. In: Megalopolis, Greece, Paleoanthropological Society Meeting, Atlanta. PaleoAnthropology, pp. A4–A5.

Blackwell, B., Sakhrani, N., Gopalkrishna, K.K., Singh, I., Harvati, K., Tourloukis, V., Panagopoulou, E., Karkanas, P., Blickstein, J.I.B., Skinner, A.R., 2018. ESR dating ungulate teeth and molluscs from Marathousa 1, Greece. Quat. Int (under review).

Dreschhoff, G.-E., 1965. Geologische Untersuchungen im Nordwesten des Beckens von Megalopolis (Peloponnes). Unpublished Diploma thesis. Reinischen Friedrich-Wilhems-Universität, Bonn.

Felletti, F., Dall'Olio, E., Muttoni, G., 2016. Determining flow directions in turbidites: an integrated sedimentological and magnetic fabric study of the Miocene Marnoso Arenacea Formation (northern Apennines, Italy). Sediment. Geol. 335, 197–215.

Giusti, D., Tourloukis, V., Konidaris, G.E., Thompson, N., Karkanas, P., Panagopoulou, E., Harvati, K., 2018. Beyond maps: patterns of formation processes at the Middle Pleistocene open-air site of Marathousa 1, Megalopolis Basin, Greece. Quat. Int (in press).

Gold, O., 1961. Vorproject Megalopolis, Band 1–5 (Textband, Anlagebände, Schichtenverzeichnisse): Lagerstaettenuntersuchungen. Bundesanstalt für Bodenforchung (Hannover) (Geozentrum Hannover Archiv).

Gold, O., 1963. General map of drillhole locations up to June 1961. Drawing 1–7244.

Hao, Q., Wang, L., Oldfield, F., Guo, Z., 2015. Extra-long interglacial in Northern Hemisphere during MISs 15-13 arising from limited extent of Arctic ice sheets in glacial MIS 14. Sci. Rep. 5, 12103.

Harvati, K., 2016. Paleoanthropology in Greece: recent findings and interpretations. In: Harvati, K., Roksandic, M. (Eds.), Paleoanthropology of the Balkans and Anatolia: Human Evolution and its Context. Springer, Netherlands, pp. 3–14.

Harvati, K., Panagopoulou, E., Tourloukis, V., Thompson, N., Karkanas, P., Athanassiou, A., Konidaris, G.E., Tsartsidou, G., Giusti, D., 2016. New Middle Pleistocene elephant butchering site from Greece. In: Paleoanthropology Society Meeting. PaleoAnthropology, Atlanta, pp. A14–A15.

Harvati, K., Panagopoulou, E., Tourloukis, V., Thompson, N., Karkanas, P., Konidaris, G.E., Athanassiou, A., Tsartsidou, G., Giusti, D., 2017. Marathousa 1: new Lower Palaeolithic elephant butchering site from the Megalopolis basin, Greece. Proc. Eur. Soc. study Hum. Evol. 6, 84.

Hillenbrand, C.-D., Kuhn, G., Frederichs, T., 2009. Record of a Mid-Pleistocene depositional anomaly in West Antartic continental margin sediments: an indicator for ice-sheet collapse? Quat. Int. 28, 1147–1159.

Hiltermann, H., Lüttig, G., 1969. Biofazies und Paläolimnologie der pliozänen und pleistozänen Seen im Megalopolis-Becken (Peloponnes). Mittl. Int. Ver. für Theoretische Angew. Limnol. 17, 306–314.

Jacobs, Z., Li, B., Karkanas, P., Tourloukis, V., Thompson, N., Panagopoulou, E., Harvati, K., 2018. Dating of Middle Pleistocene Marathousa 1 (Greece) lacustrine sediment using multiple-aliquot pre-dose multi-elevated-temperature post-infrared infrared stimulated luminescence (MET-pIRIR). Quat. Int (under review).

Kirschvink, J.L., 1980. The least square line and plane and the analysis of paleomagnetic data. R. Astronomical Soc. Geophys. J. 62, 699–718.

Karkanas, P., Tourloukis, V., Thompson, N., Giusti, D., Panagopoulou, E., Harvati, K., 2018. Sedimentology and micromorphology of the lower palaeolithic lakeshore site Marathousa 1, Megalopolis, Greece. Quat. Int (in press).

Konidaris, G.E., Athanassiou, A., Tourloukis, V., Thompson, N., Giusti, D., Panagopoulou, E., Harvati, K., 2018. The skeleton of a straight-tusked elephant (*Palaeoloxodon antiquus*) and other large mammals from the Middle Pleistocene butchering locality Marathousa 1 (Megalopolis Basin, Greece): preliminary results. Quat. Int (in press). https://doi.org/10.1016/j.quaint.2017.12.001.

Lisiecki, L.E., Raymo, M.E., 2005. A Pliocene-Pleistocene stack of 57 globally distributed benthic $\delta^{18}O$ records. Paleoceanography 20.

Löhnert, E., Nowak, H., 1965. Die Braunkohlenlagerstätte von Khoremi im Becken von Megalopolis/Peloponnes. Geol. Jahrb. 82, 847–868.
Lourens, L.J., Hilgen, F.J., Laskar, J., Shackleton, N.J., Wilson, D., 2004. The Neogene period. In: Gradstein, F.M., Ogg, J.G., Smith, A.G. (Eds.), A Geologic Time Scale 2004. Cambridge University Press, Cambridge, pp. 409–440.
Lowrie, W., 1990. Identification of ferromagnetic minerals in a rock by coercitivity and unblocking temperature proprieties. Geophys. Res. Lett. 17, 159–162.
Melentis, J.K., 1965. Die pleistozänen Cerviden des Beckens von Megalopolis im Peloponnes (Griechenland). Ann. Géologiques Des. Pays Helléniques 16, 1–92.
Nickel, B., Riegel, W., Schoenherr, T., Velitzelos, E., 1996. Environments of coal formation in the Pleistocene lignite at Megalopolis, Peloponnesus (Greece) -reconstructions from palynological and petrological investigations. Neues Jahrb. für Geol. Paläontologie 200, 201–220.
Okuda, M., van Vugt, N., Nakagawa, T., Ikeya, M., Hayashida, A., Yasuda, Y., Setoguchi, T., 2002. Palynological evidence for the astronomical origin of lignite–detritus sequence in the Middle Pleistocene Marathousa Member, Megalopolis, SW Greece. Earth Planet. Sci. Lett. 201 (1), 143–157.
Panagopoulou, E., Tourloukis, V., Thompson, N., Athanassiou, A., Tsartsidou, G., Konidaris, G.E., Giusti, D., Karkanas, P., Harvati, K., 2015. Marathousa 1: A New Middle Pleistocene Archaeological Site from Greece. project gallery Antiquity 343.
Parés, J.M., Hassold, N.J.C., Rea, D.K., van Der Pluijm, B.A., 2007. Paleocurrent directions from paleomagnetic reorientation of magnetic fabrics in deep-sea sediments at the Antarctic Peninsula Pacific margin (ODP Sites 1095, 1101). Mar. Geol. 242 (4), 261–269.
Sakorafa, V., Michailidis, K., 1997. The geology and coal petrology of a Pleistocene lignite profile at Horemi mine, Megalopolis Basin, Peloponnese (southern Greece). Int. J. Coal Geol. 33 (1), 73–91.
Scardia, G., Muttoni, G., 2009. Paleomagnetic investigations on the Pleistocene lacustrine sequence of Pianico-Sèllere (northern Italy). Quat. Int. 204 (1), 44–53.
Siavalas, G., Linou, M., Chatziapostolou, A., Kalaitzidis, S., Papaefthymiou, H., Christanis, K., 2009. Palaeoenvironment of seam I in the Marathousa lignite mine, Megalopolis basin (southern Greece). Int. J. Coal Geol. 78 (4), 233–248.
Sickenberg, O., 1975. Eine Säugertierfauna des tieferen Bihariums aus dem Becken von Megalopolis (Peloponnes, Griechenland). Ann. Géologiques Des. Pays Helléniques 27, 25–73.
Tarling, D., Hrouda, F. (Eds.), 1993. Magnetic Anisotropy of Rocks. Springer Science & Business Media, the Netherlands.
Tauxe, L., Herbert, T., Shackleton, N.J., Kok, Y.S., 1996. Astronomical calibration of the Matuyama-Brunhes boundary: consequences for magnetic remanence acquisition in marine carbonates and the Asian loess sequences. Earth Planet. Sci. Lett. 140 (1), 133–146.
Tourloukis, V., 2010. The Early and Middle Pleistocene Archaeological Record of Greece: Current Status and Future Prospects. Archaeological Studies Leiden University 23, Leiden University Press, Leiden.
Tourloukis, V., Harvati, K., 2018. The Palaeolithic record of Greece: a synthesis of the evidence and a research agenda for the future. Quat. Int. 466, 48–65.
Tourloukis, V., Thompson, N., Panagopoulou, E., Giusti, D., Konidaris, G.E., Karkanas, P., Harvati, K., 2018. Lithic artifacts and bone tools from the Lower Palaeolithic site Marathousa 1, Megalopolis, Greece: preliminary results. Quat. Int (under review).
Tzedakis, P.C., Hooghiemstra, H., Pälike, H., 2006. The last 1.35 million years at Tenaghi Philippon: revised chronostratigraphy and long-term vegetation trends. Quat. Sci. Rev. 25 (23–24), 3416–3430.
Tzedakis, P.C., Crucifix, M., Mitsui, T., Wolff, E.W., 2017. A simple rule to determine which insolation cycles lead to interglacials. Nature 542 (7642), 427–432.
van Vugt, N., de Bruijn, H., van Kolfschoten, T., Langereis, C.G., 2000. Magneto- and cyclostratigraphy and mammal-fauna's of the Pleistocene lacustrine Megalopolis basin, peloponnesos, Greece. Geol. Ultrajectina 189, 69–92.
Vinken, R., 1965. Stratigraphie und Tektonik des Beckens von Megalopolis (Peloponnes, Griechenland). Geol. Jahrb. 83, 97–148.